Design of HEAs for specific properties

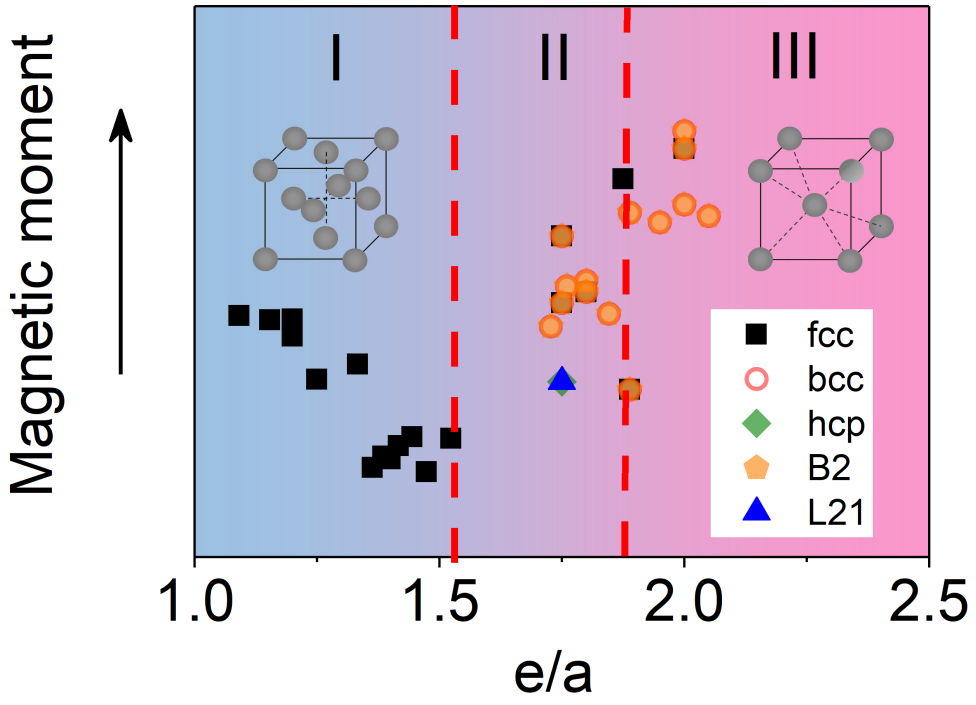

Influence of the electronic polymorphism of Ni on the classification and design of high entropy alloys

M. Calvo-Dahlborg[1,2,*], U. Dahlborg[1,2], S.G.R. Brown[2], J. Juraszek[1]

[1] Normandie Univ, UNIROUEN, INSA Rouen, CNRS, GPM, 76000 Rouen, France

[2] College of Engineering, Swansea University Bay Campus, Fabian Way, Swansea, Neath Port Talbot, SA1 8QQ, UK

*****Corresponding author: M. Calvo-Dahlborg email: monique.calvo-dahlborg@univ-rouen.fr

Abstract: According to a recent Hume-Rothery approach, the electron concentration, e/a, and the average radius can be used to identify the domain of stability of HEAs and to estimate the phases that may occur in the alloy. The present study investigates the influence of the electronic polymorphism of nickel on the efficiency of the classification and on the design of HEAs for magnetic applications. Many different compositions were used, based on 4 to 7 elements out of a total 13 different elements (Co, Cr, Fe, Ni, Al, Cu, Pd, Ti, Mn, V, Nb, Sn, Ru). Phases have been determined by X-ray and neutron diffraction as well as in some cases high energy X-ray diffraction. The e/a for the constituent elements is calculated according to Massalski. The two polymorphic electronic structure of nickel, namely $(e/a)_{Ni}=1$ or $(e/a)_{Ni}=2$ are considered. The average e/a for the alloy is calculated assuming a solid solution case. The electronic structure [Ar] $3d^9$ $4s^1$ seems to be more appropriate for the classification of HEAs. Based on a Self-Organizing Map predictions are made for the average magnetic moment at saturation for this electronic structure of Ni. Non-saturated values and data from the literature are compared with the predictions. The consequences of such results when modelling the structure and properties of Ni containing HEAs are presented, in particular the consideration of the shape and transformation of the Brillouin zone.

Keywords: HEA, e/a, phases, Ni, design, magnetism, Brillouin

1. Introduction

The term “high entropy alloys” (HEAs) was introduced in 2004 to define alloys with multiple principal elements in equimolar or near-equimolar ratios [1-2]. A new metallurgy was born by considering not one or two main elements with the others as minor additions but with all elements solidifying on an equal footing from the liquid state. In the first paper [1] stress was put on the apparent simple structure of HEAs, within a solid solution approach, having face centred cubic (*fcc*), body centred cubic (*bcc*) and hexagonal closed packed (*hcp*) structures and that these new systems exhibit extraordinary properties. In the second paper [2] the feasibility of multi-major component alloys with a large number of elements was demonstrated as well as the multiphase single structure of the CoCrFeNiMn alloy (also called the Cantor alloy) which was shown to have two fcc phases, one Fe-rich and one Fe-poor. Since 2004, many reports have determined the structures and microstructures of HEAs. It has been found that in many cases a HEA has a structure and a microstructure that are very different from ordinary alloys. Furthermore, the multi-phase single simple structure was confirmed for many of the HEAs investigated [2-9]. Following the definition of Yeh et al [1] the domain of existence of HEAs as compared to Bulk Metallic Glasses (BMGs) and intermetallics was derived using the entropy of mixing versus the atomic mismatch, *delta*, as quantitative parameters [4].

During the last 15 years, following the expectation of “extraordinary properties” mentioned by Yeh et al [1] many reports have also reviewed the potential use of these alloys for special kinds of technological applications [10-14]. The determination of the phase composition after solidification as well as their stability under external influence has been an important issue as the phase composition might strongly affect the mechanical efficiency of the alloy and thus the potential applications. Generally, *fcc* phases favour ductility and *bcc* phases favour strength and hardness. Numerous attempts using both semi-empirical and thermodynamic parameter(s) have been developed in order to understand the stability of solid solutions in some HEAs and the formation of unwanted intermetallic phases during use [15-19]. Scientific issues and challenges have been discussed including aspects of definition/terminology, phase formation, microstructure and phase stability, strengthening mechanisms, and high temperature properties, as well as the density and cost [20 - 22].

Recently a classification of HEAs was proposed using the average value of the electron concentration or number of itinerant electrons per atom (e/a) in the alloy and the average

atomic radius calculated for a 12-atoms atomic neighbourhood [23]. The importance of the number of itinerant electrons per atom to understand and predict the phases in solid solutions has been stressed as early as 1966 [24]. In [25] the use of e/a is discussed by Massalski for the determination of crystalline Hume-Rothery phases as opposed to an approach using the total number of valence electrons (VEC) (which includes the *d* electrons). In [26] Dong proposed a successful criterion based on a value of e/a and the radius for predicting approximants in quasicrystals. By applying these approaches for HEAs as solid solutions a classification and design methodology was proposed in [23]. From the variation of the average magnetic moment per atom and the hardness as a function of e/a and the 12 atoms radius, three domains could be identified in [23]: one domain containing alloys with cubic close-packed (fcc) structure, a second one containing complex and/or mixt structures and a third one containing structures belonging to the body-centered cubic (bcc) structural family. Since the work of Cantor [2] several publications have reported studies of alloys based on addition of a fifth, sixth or seventh element to a CoCrFeNi base alloy, thus replacing Mn by one, two or three other elements.

However, it is widely reported that the electronic structure of Ni can be either [Ar] $3d^8$ $4s^2$ or [Ar] $3d^9$ $4s^1$, thus, with the configuration per shell 2, 8, 16, 2 or 2, 8, 17, 1 [27]. Accordingly, Ni has one or two itinerant electrons per atom i.e. e/a for Ni can be either 1 or 2, whereas VEC is equal to 10 for both configurations. Because of the resulting influence on bonding, this duality has as consequence on the polymorphism of Ni in alloys, e.g. in amorphous alloys [28]. In the present work the influence of the polymorphism of Ni on the classification previously presented in [23] is investigated for the same set of alloys but excluding the ones not containing Ni.

2. Materials and Methods

In order to correlate the composition and the crystalline structure of phases, several different compositions were investigated. All alloys contained Co, Fe and Ni as base elements. To this base alloy one or more elements including Al, Cr, Cu, Mn, Nb, Pd, Ru, Ti, and V were added in different proportions. The crystalline structure of the phases that were found in these alloys as well as the corresponding lattice constants have earlier been determined by high resolution diffraction techniques [8, 29-32]. All investigated alloys have been produced by arc-melting and re-melted several times for homogenization and for minimization of oxides. The melts were cooled by a rapid quench in a copper mould. All diffraction studies were performed on

as-cast materials. For comparison, a few results on alloys containing refractory elements taken from the literature have also been included for illustrative purposes [10].

When aiming to classify alloys according to their phase content one immediately faces a problem. How are the phases determined? Diffraction techniques are most commonly used but the different diffraction techniques have different resolutions. The investigations of a CoCrFeNiPd alloy clearly illustrates this [8]. This alloy, in as-cast condition originally, was determined from laboratory X-ray measurements (XRD) to be monophase with a simple fcc structure. Neutron diffraction measurements (ND) later suggested the alloy to be at least two-phase while high-energy X-ray diffraction (HEXRD) found it to be at least four-phase. All phases were of simple fcc structure. It can thus be concluded that this alloy is multiphase but single-structured [32]. This has been found to be the case for most HEAs. Moreover, the CoCrFeNiMn was indeed reported to be two-phase in the original work of Cantor [2].

In the present work results obtained using the three above-mentioned experimental diffraction techniques are used to classify alloys according to their structural content. The ND measurements were performed on the D20 diffractometer at Institute Laue-Langevin (ILL), Grenoble (France), the HEXRD measurements on the ID22 diffractometer at the European Synchrotron Research Facility (ESRF), Grenoble (France) and the standard XRD measurements were performed with a Cobalt source at GPM, University of Rouen, France. As all samples were found to have a pronounced texture, they were rotated during the measurements, whenever possible. The structure and the lattice constants of the phases present in the alloys were determined by a refinement procedure.

Magnetic characteristics of the samples were determined by measuring the average magnetic moment per atom using a MPMS-5XL SQUID magnetometer as a function of applied magnetic field and temperature.

As in [23], Self-Organising Map (SOMs) [33-36] were determined to try to predict the existing phases as well as the average magnetic moment at 5K at saturation, $M_{5K\text{-}Sat}$, in a HEA according to its e/a and radius values. SOMs are commonly used to reveal trends in multiple parameter characterization in various domains. In [23] the applicability of a standard SOM to HEAs with 15 parameters was demonstrated. In the present work only three parameters were considered, namely the e/a value of the alloy, its average radius and $M_{5K\text{-}Sat}$. However, in the current work a ‘visualisation-induced self-organising map’ (ViSOM) has been used [36]. The ViSOM procedure followed here is a modification of the standard SOM algorithm used in [23] and is described below.

The 3 parameters are defined as the vector ***ALLOY*** and are stored in a Nx3 array, N being the number of compositions. SOMs provide a methodology for representing such data in a lower dimensional format, usually in the form of a 2D map [33]. SOMs are widely described in the general literature so only a brief overview is provided here [33-36]. Initially each parameter in the vector ***ALLOY*** is individually scaled from 0 to 1 (e.g. all average radii are scaled between 0 and 1 etc.). A training vector is then selected. The training vector consists of a subset ***SUB*** containing the 3 parameters from ***ALLOY***. ***SUB*** is represented by a 20x20 grid of nodes, which forms the map, where each node initially possesses its own uniformly distributed random values, from U(0,1), for each of the 3 parameters. Construction of the SOM proceeds by repetition of the following 'time' steps, *t*.

1: Randomly select an alloy (1 to N), $\mathbf{ALLOY_x}$.

2: Determine the node that most closely matches the chosen alloy, $\boldsymbol{SUB_w}$, i.e. the node that minimizes the expression, $\|\boldsymbol{SUB}_i - \boldsymbol{ALLOY}_x\|$. This 'winning node' is now defined as the **best matching unit** or **BMU**.

3: Next, the neighbourhood of the **BMU** is determined. The neighbourhood is made up of those nodes, $\boldsymbol{SUB_n}$, that are within a fixed distance of the **BMU**. This fixed distance decreases as more steps are performed so that **BMU** neighbourhoods become smaller as t increases.

4: The winning node is updated in the standard way using

$$\boldsymbol{SUB}_w^t = \boldsymbol{SUB}_w^{t-1} + \theta(t)\,\eta(w,n,t-1)\,(\boldsymbol{ALLOY}_x - \boldsymbol{SUB}_w^{t-1}) \quad (1)$$

5: In the neighbourhood nodes, *n*, the value of $\boldsymbol{SUB_n}$ is adjusted to move towards $\mathbf{ALLOY_x}$ using a modified form of equation 1,

$$\boldsymbol{SUB}_n^t = \boldsymbol{SUB}_n^{t-1} + \theta(t)\,\eta(w,n,t-1)$$
$$\left((\boldsymbol{ALLOY}_x - \boldsymbol{SUB}_w^{t-1}) + (\boldsymbol{SUB}_w^{t-1} - \boldsymbol{SUB}_n^{t-1})\left(\frac{\boldsymbol{d}_{wn} - \boldsymbol{\Delta}_{wn}\lambda}{\boldsymbol{\Delta}_{wn}\lambda}\right)\right) \quad (2)$$

where $\boldsymbol{d}_{wn}$ is the distance between the nodes in the data space, $\boldsymbol{\Delta}_{wn}$ is the distance between the nodes on the unit grid, λ is a prespecified resolution parameter, $\eta(w,n,t\text{-}1)$ is a neighbourhood function that decreases monotonically with distance and $\theta(t)$ is a weighting function, the so-called learning rate, which decreases linearly with increasing time steps, *t*.

6: The process is then repeated N times until the fixed distance defining the **BMU** neighbourhood becomes just one node.

Once this process is finished the **BMU** for each alloy is then determined and the alloys are placed on the map at their **BMU** locations. The ViSOM is very similar to the standard SOM

approach but it constrains the contraction within the updating neighbourhood and unlike standard SOM it provides quantitative inter-point distances on the final map.

3. Results and discussion

3.1. Comparison of the distribution of the existing phases in the {e/a1;r] and {e/a2;r} frames

From the two previous uses of e/a to predict crystalline phases in alloys, e.g. the Hume Rothery phases [24,25] and the approximants of quasicrystals [26], and to some extent also their physical properties, two other requirements were needed: 1) to combine e/a calculation with the calculated average radius of the elements in the alloy and 2) the validity of the solid solution approximation. The last condition is solved by both the definition of HEAs by Yeh [1] and the classification of HEAs as a function of the entropy of mixing and the mismatch [4]. As pointed out in [37] the exact "atomic diameter" of an element is always difficult to define. The atomic distances used in Hume-Rothery approach are defined [38] as the closest distances of approach of atoms in the crystals of the elements. The radii given by Teatum in [39] were chosen for the classification in [23] as they are reported for a coordination number of 12. Furthermore, the Teatum radii were calculated from a combination of the observed interatomic distances in fcc, hcp and bcc structures. Assuming in a first approximation that all constituent phases can be considered as solid solutions, all characteristics have been calculated from linear combinations of the characteristics of the individual constituting elements weighted by their atomic percentages. Providing error bars for all of the calculated data is acknowledged as challenging as all quantities are obtained by using commonly available databases of physics, such as the radius for bcc, fcc and hcp structure [39].

The alloy average values of e/a have been calculated as in [23] according to Massalski [25], that is e/a is equal to the electrons of the outside layer. For example, in the case of Zn, with [Ar] $3d^{10}$ $4s^2$ as electronic structure, there are 2 electrons in the outside layer and 10 d electrons. Thus, e/a=2. In the following e/a2 or eoa2 will stand for the e/a calculated with the value 2 for Ni and e/a1 or eoa1 the one for a value of 1. In [23] the e/a values are e/a2. In order to investigate the influence of the polymorphism of nickel for the case of HEAs Fig. 1 presents the variation of e/a1 and e/a2 as a function of the average radius, with an indication of the phases identified by diffraction.

It can be seen that for both choices of e/a the alloys containing solely fcc phases are found at low e/a values and that those with bcc phases are found especially at large e/a and r values.

It is clearly seen that there is a range of e/a values in which one finds alloys consisting of one or several fcc phases (Domain I), another range within which one finds alloys consisting of mainly bcc phases (Domain III) and a third range in which alloys consisting of phases with more complex structures are found (Domain II). For both configurations of Ni (Fig. 1a and b) the three Domains identified to separates the three types of alloys, namely fcc, mixed and bcc, are indicated by the horizontal bars.

In Fig.1a the three Domains give a good separation between the three types of alloys: the alloys in Domain I are only of fcc or hcp type. In Domain III they are of bcc type. A large amount of alloys are observed in Domain II at large radius with bcc type. The data for these alloys come from the literature [10] and only one phase was mentioned, no indication being given on the other minor phases. In Fig. 1b, although Domain II contains only bcc type alloys, it was not possible to have Domain I containing only fcc or hcp alloys. Domain II, for both Fig. 1a and 1b, contains alloys for which the phases identified are of mixed type. This classification is very useful to clearly distinguish the domain of occurrence of intermetallic phases which will evolve and/or stabilize upon heating leading to deterioration of specific HEAs properties.

From observation of Fig. 1, a and b, the following conclusions can be drawn:

1) The domain borders identified for e/a2 do not properly separate alloys according to the phases present. There is no clear division between fcc, mixed and bcc types.
2) The value 1 for Ni e/a ([Ar] 3d9 4s1) seems to be more suitable to obtain a correct separation of the three Domains:

   Domain I: e/a1< 1.53: fcc,
   Domain II 1.53< e/a1 < 1.88: mixed phases,
   Domain III e/a1 > 1.88: bcc
3) Domain II contains phases of mixed types and/or intermetallic phases.

Accordingly, the e/a1 values were used in the following.

3.2. Mapping of the experimental results

The target physical property used for a classification based on e/a and r in [23] was the value of the measured average magnetic moment per atom at saturation at 5K, $M_{5K\text{-}Sat}$. This value is obtained from the variation of M as a function of the applied magnetic field as presented in Fig. 2 for a Pd HEA alloy. The variation of $M_{5K\text{-}Sat}$ is shown as a function of e/a1 in Fig. 3. The vertical bars indicate the separation between the identified domains in Fig. 1a.

As expected from [24] and [25] for Hume-Rothery crystalline phases, and already shown with less resolution as a function of e/a2 in [23], there is a significant variation of $M_{5K\text{-}Sat}$ as a function of the electronic structure of the corresponding HEAs. The set of values presented in Fig. 3 has been used in the following to build a Self-Organising Map and to derive a prediction program for $M_{5K\text{-}Sat}$ for any HEA, given its e/a1 and its radius.

As already used in [23] with e/a2, the Self-Organising Map (SOM) approach can be used to get a picture of several combined parameters. Fig. 4, a to c presents the results arising from the selective choice of e/a, r and M. The maps show the locations of the different alloys (labelled as L1, L2 etc.). It can be observed is that the alloys are always at the same positions on the maps shown in figures 4, a to c. In each figure the thick doted lines represent the values of the frontiers between domains as identified in Fig. 1a, namely e/a1= 1.53 and 1.88 for the alloys. The representation produced by the SOM and the identified domains in figure 4a, b and c, corresponding respectively to *e/a*, r and *M*, are correlated to what is observed in Fig. 3: Alloys with e/a1<1.53 of Domain I are in the blue regions of the three figures, alloys with e/a1>1.88 of Domain III in the red regions.

It is important to stress here that contrary to the {e/a;r} approach based on considerations on the electronic structure of alloys as detailed in [24,25], the SOM approach belongs to data mining.

3.2. Comparison of the prediction of the average magnetic moment per atom with e/a1, design maps

In [23] Self-Organizing Maps were built and used to predict the existing phases of HEAs according to their e/a and radius values. Whereas the values 2 was used for Ni in [23], the e/a1 values of Fig. 3 are used here to make another prediction program, PredictorE1. Two sets of alloys have been used for comparison with experiments:

i) alloys for which no saturation of magnetization could be recorded on M(H) loops until 2T (Fig. 6).

For clarity, Fig. 5 gives a representative example of the variation M(H) of the average magnetic moment per atom, M, as a function of the applied field H for such alloys. In Fig. 2, the alloy has reached a saturated magnetic state and a value at saturation, $M_{5K\text{-}sat}$, can be estimated. In Fig. 5, no saturation could be observed in the interval of the experiment. Thus, the reported experimental value of M in is just the maximum value at 5K for a maximum field value of μ_0=2 T.

Fig. 6 present the values obtained through the PredictorE1 in the same frame as Fig. 3, the map data being represented by small stars, the non-saturated values by large down triangles and the results of PredictorE1 with indication of the phases present.

It can be observed the following:

1) The non-saturated values are outside the range of the curve from Fig.2 and much lower.
2) The values predicted by the PredictorE1 program are all located within the set of values presented in Fig.2.
3) As would be expected, these values are all above the values determined for the non-saturated samples.
4) The identified phases correspond to the three Domains identified before.

Again, it should be stressed that the PredictorE1 program is based on data mining approach whereas the value at saturation is a magnetic characteristic.

ii) alloys from literature produced in the same way [10].

Fig. 7 presents the values of $M_{5K\text{-}Sat}$ predicted for alloys for which the identified phases were reported in the literature [10]. The predicted values for these alloys are within the range of values of the map presented in Fig. 2. Furthermore, the values are for most within the Domain corresponding to the identified phases. It should be noted that details on the identification of the phases was not always given in the literature. It was thus impossible to check the accuracy of the determination and/or whether other minor phases were present.

The summary of observations from both Fig. 6 and 7 are the following:

1) As expected, the predicted values for saturation of the non-saturated values are within the range of the map and within the Domains corresponding to the identified phases.
2) The predicted values for samples from the literature for which the identified phases were reported are within the range of the map and within the Domains corresponding to the identified phases.

3.3. Brillouin zone

The influence of the electron concentration e/a is known since [24] to determine the phases present in an alloy following the 3 Hume-Rothery rules. In the iconic works [40,41] Jones is showing for a large series of binary systems that the value e/a=1.85 is identified as the change in the c/a ratio of the hcp structure and linked to the overlapping of some faces of the Brillouin zone. The same observation has been used in [26] for the approximants of quasicrystals.

In the case of HEAs, the Teatum radius associated with the electron concentration e/a1 in the solid solution approximation is showing that the phases present as well as certain properties can be similarly predicted. The value 1.85 corresponds to a e/a1 value equal to 1.65. In order to investigate if such value has a meaning in the case of HEAs a characteristic related to an abrupt change of property was chosen: the magnetic transition as recorded in an M(T) curve by SQUID. Fig. 8 present the variation of T_m as a function of e/a1. T_m is determined by the zero point of the second derivative of the M(T) curve. Thus, it is not the Curie temperature defining the start of the zero magnetization. Two lines were drawn between the fcc points and between the bcc points. The value 1.65 corresponds to the intersection between the two lines.

From the observation of Fig. 8 it is clear that the value e/a1=1.65 is also corresponding to an abrupt change in the phases present in HEAs. Moreover, similarly to what has been the case for the design and interpretation of quasicrystals the Brillouin zone has to be introduced in calculations and modelling of HEAs in addition to the electron concentration e/a and the radius.

4. Conclusions

1) When an HEA composition contains nickel its electronic structure or [Ar] $3d^9$ $4s^1$ should be considered instead of [Ar] $3d^8$ $4s^2$.

Thus, the domains defining the presence of phases are the following:

Domain I: e/a (Ni=1)< 1.53: fcc,

Domain II 1.53< e/a (Ni=1) < 1.88: mixed phases,

Domain III e/a (Ni=1) > 1.88: bcc.

2) A Self-Organizing Map approach can be built to predict phases present in a HEA according to its e/a and radius values.

3) For the [Ar] $3d^9$ $4s^1$ electronic structure of Ni, the experimental and the predicted values are consistent within the range of the map.

4) Based on this map the average magnetic moment at saturation can be predicted for HEAs as well as the Domain defining the presence of particular phases. This last result is of great importance and potential use for future applications involving the magnetic properties of HEAs

5) As has been the case for the design and understanding of Hume Rothery phases and quasicrystals the Brillouin zone of HEA systems has to be investigated in their calculations and modelling.

Acknowledgments:

SGRB acknowledges the support of the Welsh Government and Welsh European Funding Office in the Combinatorial Metallurgy (COMET) Smart Expertise Project. The samples have been prepared within the FP7 European project AccMet NMP4-LA-2011-263206.

References

[1] J.W. Yeh, S.K. Chen, S.J. Lin, J.Y. Gan, T.S. Chin, T.T. Shun, C.H. Tsau, S.Y. Chang, Nanostructured high-entropy alloys with multiple principal elements: novel alloy design concepts and outcomes, Adv. Eng. Mater. 6 (2004) 299-303.

[2] B. Cantor, I.T.H. Chang, P. Knight, A.J.B. Vincent, Microstructural development in equiatomic multicomponent alloys, Mater. Sci. Eng. A 375-377 (2004) 213-218.

[3] O.N. Senkov, J.D. Miller, D.B. Miracle, C. Woodward, Accelerated exploration of multi-principal element alloys with solid solution phases, Nature Communications 6 (2015) 6529.

[4] S. Guo, Q. Hu, C. Ng, C.T. Liu. More than entropy in high-entropy alloys : Forming solid solutions or amorphous phase. Intermetallics 41 (2013) 96-103.

[5] S. Singh, N. Wanderka, B.S. Murty, U. Glatzel, J. Banhart, Decomposition in multi-component AlCoCrCuFeNi high-entropy alloy, Acta Mater. 59 (2011) 182–190.

[6] A. Manzoni, H. Daoud, R. Völkl, U. Glatzel, N. Wanderka, Phase separation in equiatomic AlCoCrFeNi highentropy alloy, Ultramicroscopy 132 (2013) 212–215.

[7] Y.P Wang, B.S. Li, H.Z. Fu, Solid solution or intermetallics in a high-entropy alloy, Adv. Eng. Mater. 11 (2009) 641–644.

[8] U. Dahlborg , J. Cornide, M. Calvo-Dahlborg, T.C. Hansen, A. Fitch, Z. Leong, R. Goodall. Structure of some CoCrFeyNi and CoCrFeNiPdx multicomponent HEA alloys by diffraction techniques. J. Alloys and Compounds 681 (2016) 330-341.

[9] S. Guo, Q. Hu, C. Ng, C.T. Liu, More than entropy in high-entropy alloys: Forming solid solutions or amorphous phase, Intermetallics 41 (2013) 96-103.

[10] M.C. Gao, J.W. Yeh, P.K. Liaw, Y. Zhang Y. High-Entropy alloys: Fundamentals and applications, Springer, 2016.

[11] Y. Zhang, T.T Zuo, Z. Tang, §§M.C Gao, K.A. Dahmen, P.K. Liaw, Z.P. Lu, Microstructures and properties of high-entropy alloys, Prog. Mater. Sci. 61 (2014) 1-93.

[12] D.B. Miracle, O.N. Senkov, A critical review of high entropy alloys and related concepts, Acta Materialia 122 (2017) 448–511.

[13] D.B. Miracle, J.D. Miller, O.N. Senkov, C. Woodward, M.D. Uchic, J. Tiley, Exploration and Development of High Entropy Alloys for Structural Applications, Entropy 16 (2014) 494-525.

[14] O.N. Senkov, J.D. Miller, D.B. Miracle, C. Woodward, Accelerated exploration of multi-principal element alloys with solid solution phases, Nature Communications 6 (2015) 6529.

[15] F. Otto, Y. Yang, H. Bei, E.P. George, Relative effects of enthalpy and entropy on the phase stability of equiatomic high-entropy alloys, Acta Mater. 61 (2013) 2628–2638.

[16] M.G. Poletti, L. Battezzati, Electronic and thermodynamic criteria for the occurrence of high entropy alloys in metallic systems, Acta Mater. 75 (2014) 297-306.

[17] I. Toda-Caraballo, P.E.L. Rivera-Díaz-del-Castillo, A criterion for formation of high entropy alloys based on lattice distortion. Intermetallics 71 (2016) 76-87.

[18] R. Kozak, A.S. Sologubenko, W. Steurer. Single-phase high-entropy alloys – an overview. Zeitschrift fuer Kristallographie Crystalline Materials, 230 (2015) 55-68.

[19] D.J. M. King, S.C. Middleburgh, A.G. McGregor, M.B. Cortie. Predicting the formation and stability of single phase high-entropy alloys. Acta Mater, 104 (2016) 172-179.

[20] X. Yang, Y. Zhang, Prediction of high-entropy stabilized solid-solution in multi-component alloys, Materials Chemistry and Physics, 132 (2012) 233–238.

[21] M.H. Tsai, J.W. Yeh, High-entropy alloys: A critical review, Mater. Res. Lett. 2-3 (2014) 107-123.

[22] Z.P Lu, Z.F Lei, H.L. Huang, S.F. Liu, F. Zhang, D.B. Duan, P.P. Cao, Y. Wu, X. Liu, H. Wang, Deformation behavior and toughening of High-Entropy Alloys, Acta Metall Sin, 54 (2018) 1553-1566.

[23] M. Calvo-Dahlborg et S. G. R. Brown. Hume-Rothery for HEA classification and self-organizing map for phases and properties prediction. J. Alloys and Compds 724 (2017) 353-364.

[24] Structure of metals, third edition. C.S. Barrett, T.B. Massalski. McGraw-Hill Eds. 1966. P. 306-379.

[25] T.B. Massalski, Comments Concerning Some Features of Phase Diagrams and Phase Transformations, Materials Transactions 51 (2010) 583-596.

[26] Chuang Dong, The concept of the approximants of quasicrystals, Scripta Materialia 33 (1995) 239-243.

[27]Scerri, Eric R., The periodic table: its story and its significance, Oxford University Press, 2007 (ISBN 0-19-530573-6), p. 239–240.

[28]D. S. Lashmore, L. H. Bennett, H. E. Schone, P. Gustafson, and R. E. Watson, Polymorphism of Nickel-Phosphorus Metallic Glasses. Phys. Rev. Lett. 48 (1982) 1760-1763.

[29]J. Cornide, U. Dahlborg, Z. Leong, L. Asensio Dominguez, J. Juraszek, S. Jouen, T. Hansen, R. Wunderlich, Chambreland S, Todd I, Goodall R and Calvo-Dahlborg M 2015 The Minerals, Metals & Materials Society (2015) in TMS2015 Supplemental Proceedings, John Wiley & Sons, Inc., Hoboken, NJ, USA. doi: 10.1002/9781119093466.ch139. Structure and properties of some CoCrFeNi-based high Entropy alloys.

[30] Dahlborg U, Cornide J, Calvo-Dahlborg M, Hansen T C, Leong Z, Asensio Dominguez L, Chambreland S, Cunliffe A, Goodall R and Todd I 2015 Acta. Phys. Polonica A 128 552. Crystalline structures of some High Entropy Alloys obtained by Neutron and X-ray diffraction,

[31]Cornide J, Calvo-Dahlborg M, Chambreland S, Asensio Dominguez L, Leong Z, Dahlborg U, Cunliffe A, Goodall R and Todd I 2015 Acta Phys. Polonica A 128 557. Combined Atom Probe Tomography and TEM investigations of CoCrFeNi, CoCrFeNi-Pdx (x=0.5, 1.0, 1.5) and CoCrFeNi-Sn.

[32] Calvo-Dahlborg M, Cornide J, Dahlborg U, Chambreland S, Hatton G D, Fones A, 2017 Solid State Phenomena 257 72. Structural and microstructural characterization of CoCrFeNiPd High Entropy Alloys.

[33] T. Kohonen, Self-Organized Formation of Topologically Correct Feature Maps. Biol. Cybern. 43 (1982) 59-69.

[34] E. Alhoniemi, J. Himberg, J. Hollmen, S. Laine, P. Lehtimaki, K. Raivio, T. Simila, O. Simula, M. Sirola, M. Sulkava, J. Tikka, J. Vesantoc, Biennial report 2002-2003. K. Puolamäki, L. Koivisto (Eds), Otaniemi, Helsinki University of Technology. Laboratory of Computer and Information Science, 2004, pp 171-177.

[35] J. Ong, S.S. Raza Abidi, Data Mining Using Self-Organizing Kohonen maps: A Technique for Effective Data Clustering & Visualisation. International Conference on Artificial Intelligence (IC-AI'99), June 28-July 1 1999, Las Vegas.

[36] Hujun Yin, IEEE Trans. On Neural Networks, 13, 1, 2002, 237-243.

[37] W. Hume-Rothery, G.W. Mabbot, Channel Evans K.M. The freezing points, melting points and solid solubility limits of the alloys of silver and copper with the elements of the B-sub-groups, Phil. Trans. Royal soc. London A 232 (1934) 1-97.

[38] W. Hume-Rothery, Atomic diameters, atomic volumes, and solid Solubility relations in alloys, Acta Metallurgica 14 (1966) 17-20.

[39] E.T. Teatum, K.A. Gschneidner Jr, J.T. Waber, Compilation of calculated data useful in predicting metallurgical behavior of the elements in binary alloy systems. Report 1968 LA-4003. UC-25. Metals, Ceramics and Materials. TID-4500, Los Alamos Scientific Laboratory. In Physical Metallurgy, vol. 1. R.W.Cahn, P. Haasen (Eds.) Elsevier, 1996.

E.T. Teatum, K.A. Gschneidner Jr., J.T. Waber, 1968. Report LA-4003. UC-25. Metals, Ceramics and Materials.TID-4500, Los Alamos Scientific Laboratory.

[40] H. Jones, Applications of the Bloch theory to the study of alloys and of the properties of bismuth. Proc. Roy. Soc. (London) A147 (1934) p.396-412.

[41] H. Jones, The effect of electron concentration on the lattice spacings in magnesium solid solutions. Phil Mag 41 (1950) p.663-670.

Figure captions

Fig. 1: a) e/a1 b) e/a2 as a function of the average Teatum radius. The symbols indicate the types of phases identified by diffraction: ■ fcc, ○ bcc, Λhcp, ▲L21, B2, + Sigma or Tetragonal, mixed, not determined. The horizontal bars determine the domains I, II and III containing fcc, and bcc phases.

Fig. 2: Representative example of an HEA exhibiting ferromagnetic properties with saturation of magnetization on the M(H) loops at 5 K.

Fig. 3: Average magnetic moment per atom at saturation at 5K, M_{5K}, as a function of e/a1. The symbols indicate the types of phases identified by diffraction: ■ fcc, ○ bcc, Λhcp, ▲L21, B2, not determined. The horizontal bars determine the domains I, II and III containing fcc, and bcc phases.

Fig.4: SOM results for (a) e/a, (b) r, (c) $M_{5K\text{-}Sat}$ when **SUB** = e/a and r. On the colour scale red corresponds to the maximum value and blue to the minimum.

Fig. 5: Representative examples of M(H) curves for a Ru HEA for which no saturation state was observed until 2T.

Fig. 6: Average magnetic moment per atom at 5K, M_{5K}, as a function of e/a1. (ξ) Values of the map from Fig. 2. (B) Non saturated values as measured. Values after PredictorE1: The symbols indicate the types of phases identified by diffraction: ■ fcc, ○ bcc, Λhcp, ▲L21, B2, not determined. The horizontal bars determine the domains I, II and III containing fcc, and bcc phases.

Fig. 7: Average magnetic moment per atom at 5K, M_{5K}, as a function of e/a1 for alloys in the literature. (ξ) Values of the map from Fig. 2. Values after PredictorE1: The symbols indicate the types of phases identified by diffraction: ■ fcc, ○ bcc, Λhcp, ▲L21, B2, not determined. The horizontal bars determine the domains I, II and III containing fcc, and bcc phases.

Fig. 8: The temperature of magnetic transition T_m as a function of e/a1 for the alloys of Fig. 3 for which it was possible to record until 400K. The symbols indicate the types of phases identified by diffraction: ■ fcc, ○ bcc,T, B2, not determined.

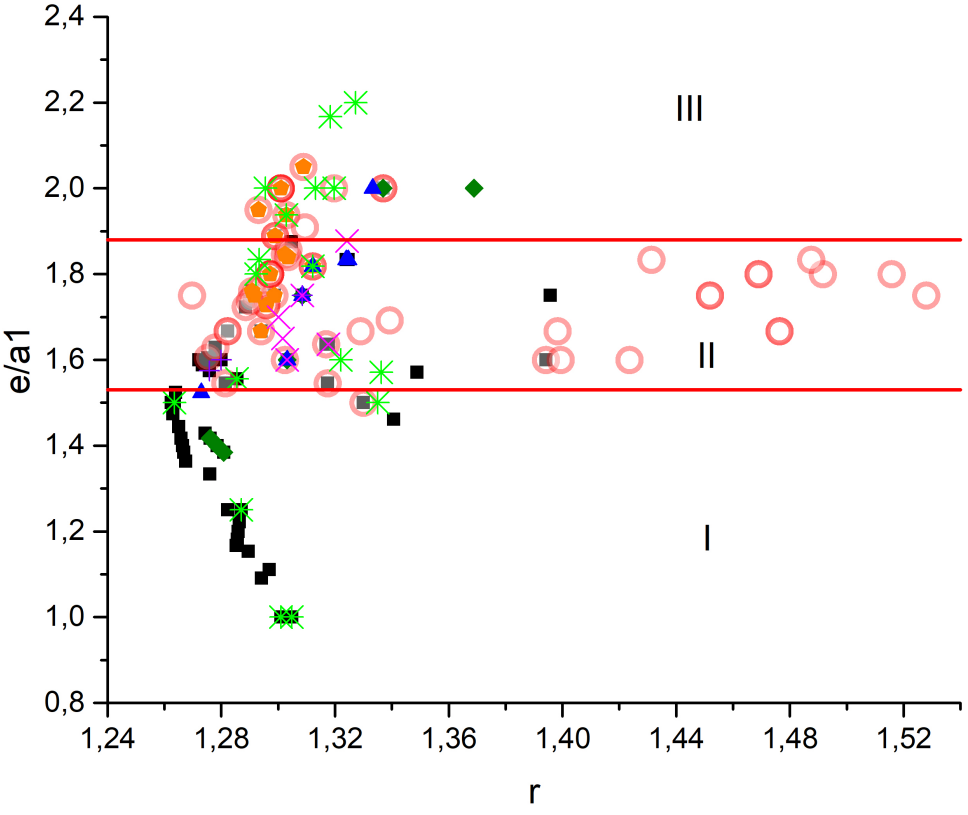
2,4
2,2
2,0
1,8
1,6
1,4
1,2
1,0
0,8
e/a1
1,24
1,28
1,32
1,36
1,40
1,44
1,48
1,52
r
III
II
I

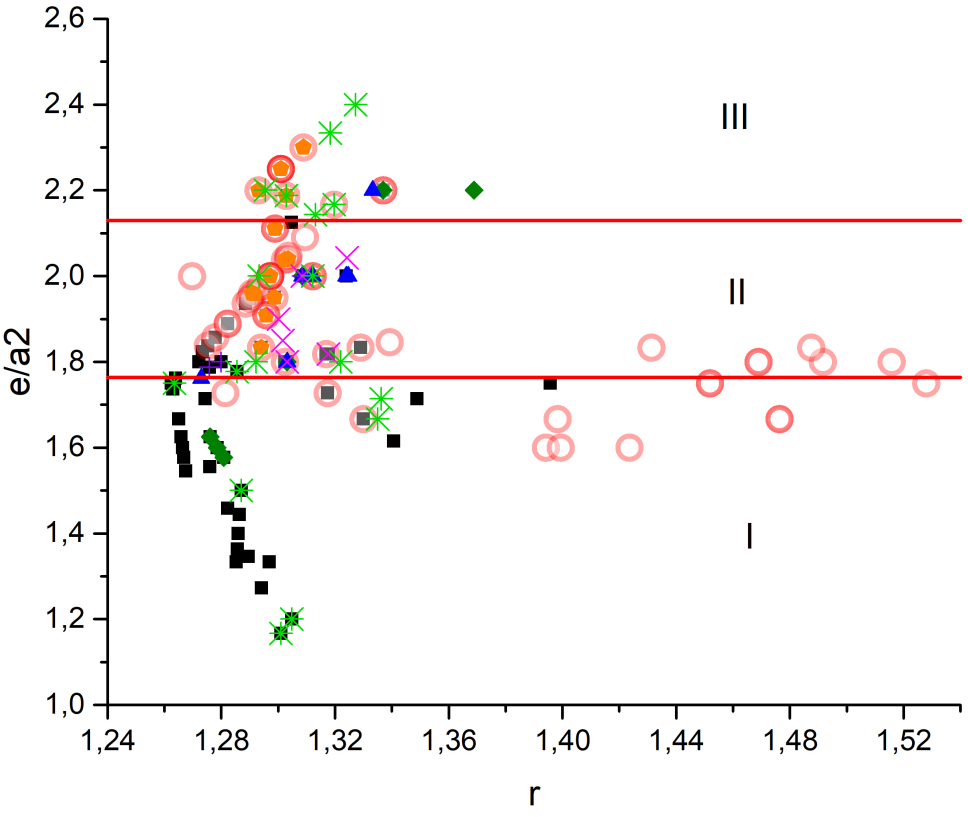
2,6
2,4
2,2
2,0
1,8
1,6
1,4
1,2
1,0
e/a2
1,24
1,28
1,32
1,36
1,40
1,44
1,48
1,52
r
III
II
I

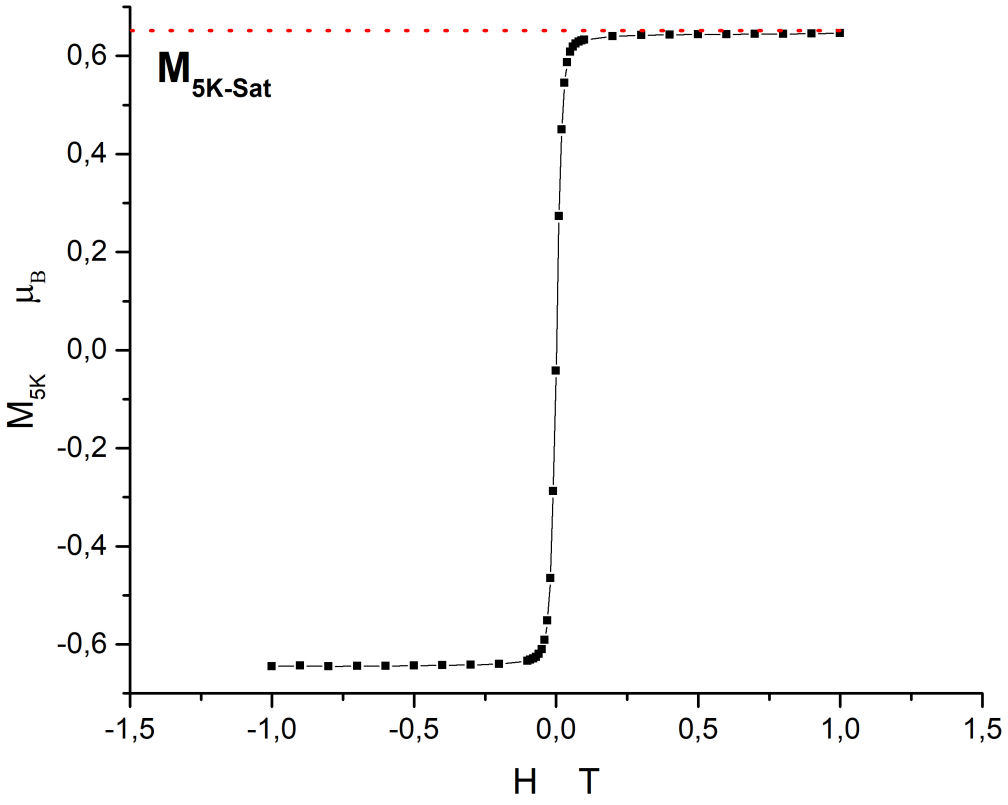

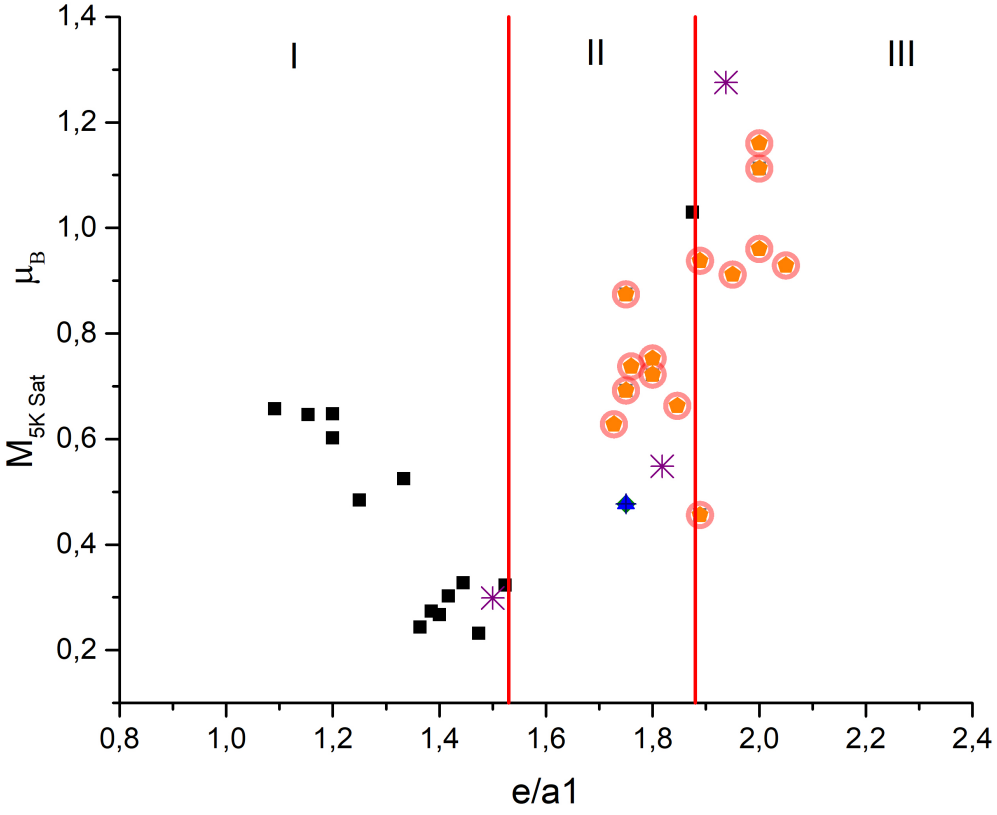
I
II
III
1,4
1,2
1,0
0,8
0,6
0,4
0,2
$M_{5K\ Sat}$ μ_B
0,8
1,0
1,2
1,4
1,6
1,8
2,0
2,2
2,4
e/a1

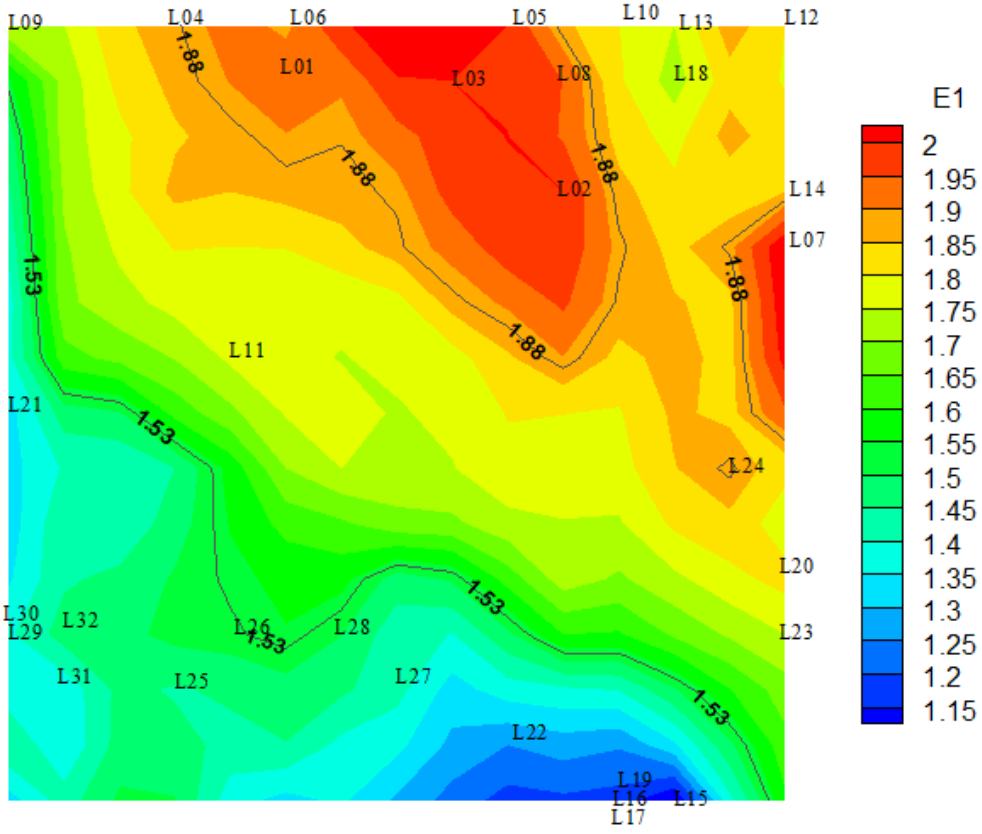
L09
L04
L06
L05
L10
L13
L12
L01
L03
L08
L18
L02
L14
L07
L11
L21
L24
L20
L30
L29
L32
L26
L28
L23
L31
L25
L27
L22
L19
L16
L15
L17
1.88
1.53
E1
2
1.95
1.9
1.85
1.8
1.75
1.7
1.65
1.6
1.55
1.5
1.45
1.4
1.35
1.3
1.25
1.2
1.15

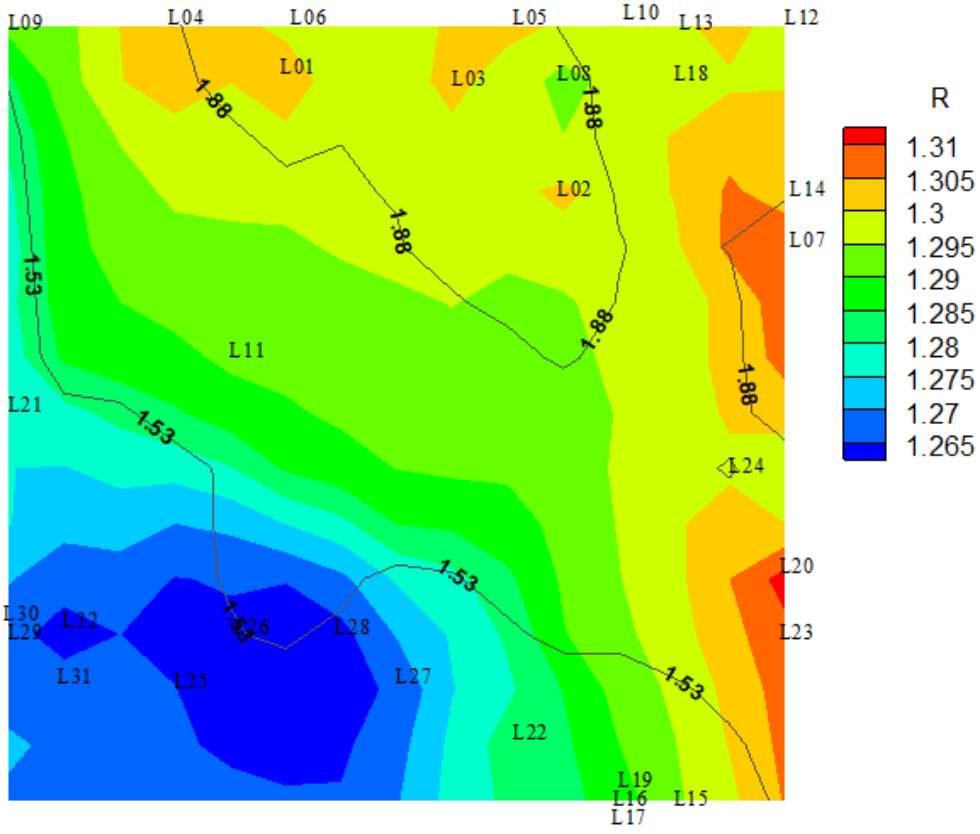
L09
L04
L06
L05
L10
L13
L12
L01
L03
L08
L18
L02
L14
L07
L11
L21
L24
L20
L23
L30
L29
L32
L26
L28
L31
L25
L27
L22
L19
L16
L17
L15
1.88
1.53
R
1.31
1.305
1.3
1.295
1.29
1.285
1.28
1.275
1.27
1.265

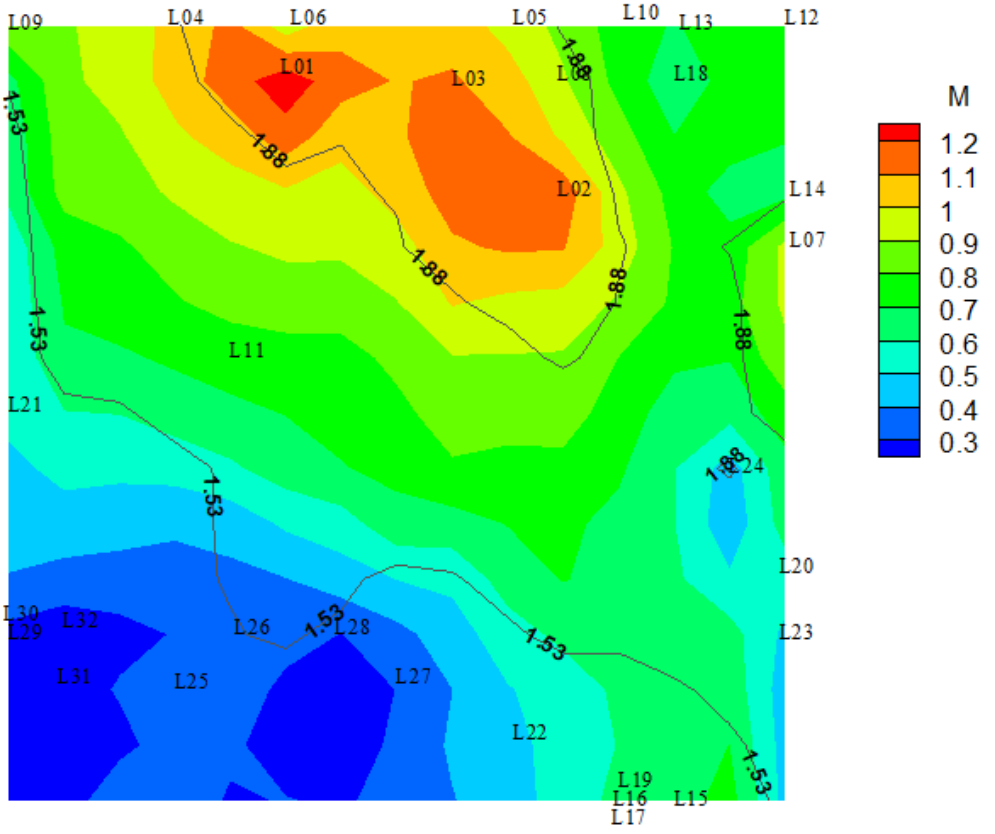
L09
L04
L06
L05
L10
L13
L12
L01
L03
L08
L18
L02
L14
L07
L11
L21
L24
L20
L30
L29
L32
L26
L28
L23
L31
L25
L27
L22
L19
L16
L15
L17
1.53
1.88
M
1.2
1.1
1
0.9
0.8
0.7
0.6
0.5
0.4
0.3

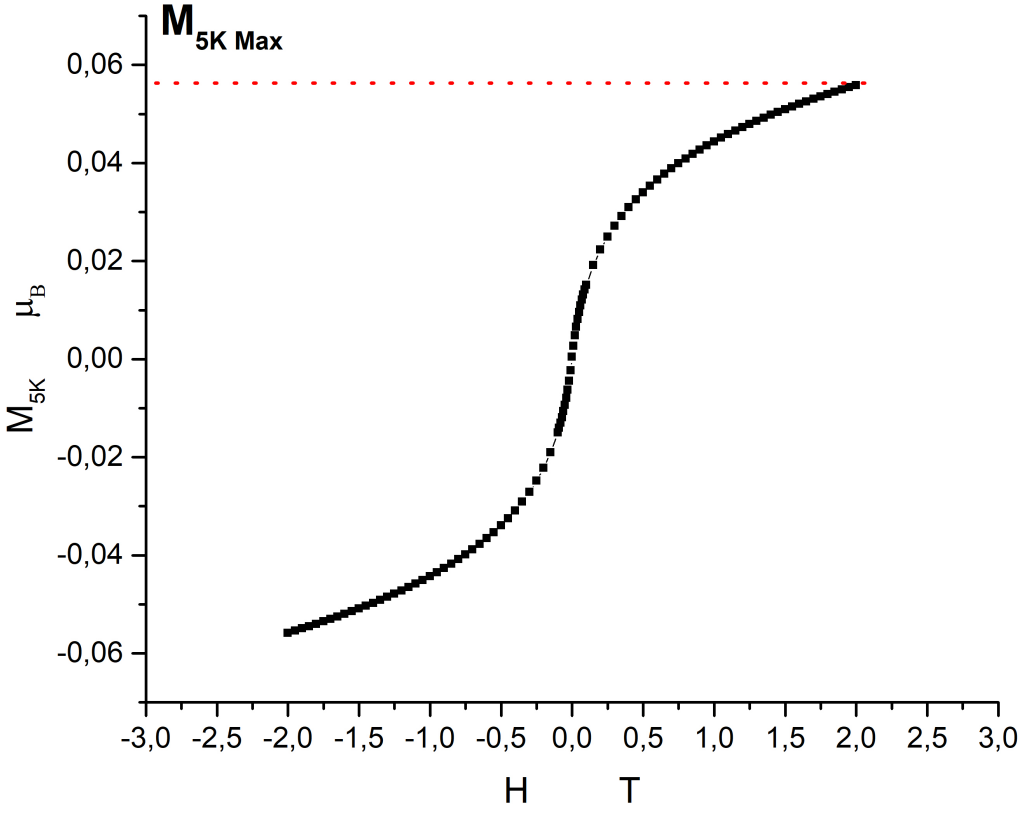
M5K Max
0,06
0,04
0,02
0,00
-0,02
-0,04
-0,06
M5K μB
-3,0 -2,5 -2,0 -1,5 -1,0 -0,5 0,0 0,5 1,0 1,5 2,0 2,5 3,0
H T

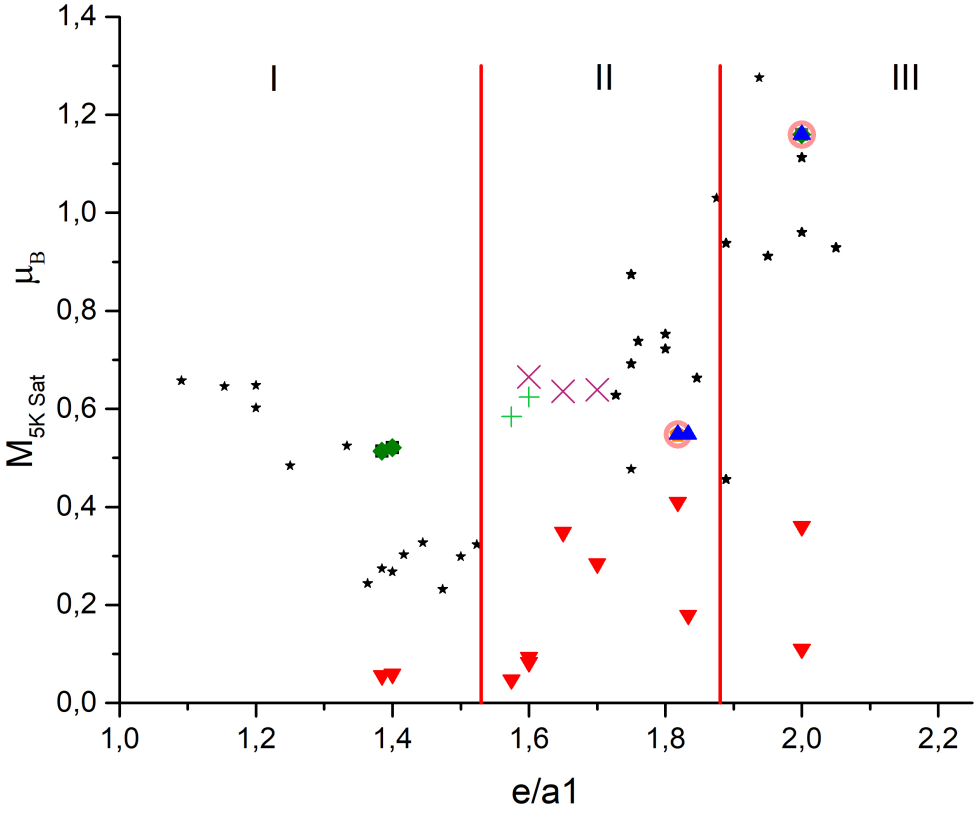
I
II
III
$M_{5K\ Sat}$ μ_B
e/a1
1,4
1,2
1,0
0,8
0,6
0,4
0,2
0,0
1,0
1,2
1,4
1,6
1,8
2,0
2,2

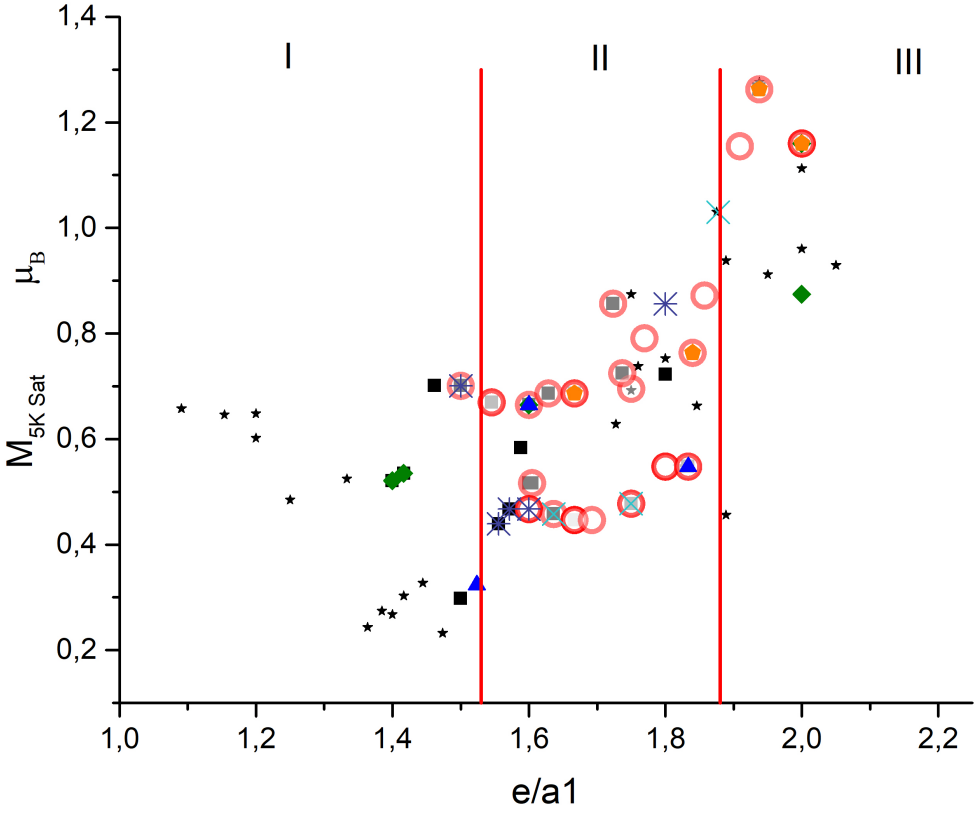
I
II
III
1,4
1,2
1,0
0,8
0,6
0,4
0,2
$M_{5K\ Sat}$ μ_B
1,0
1,2
1,4
1,6
1,8
2,0
2,2
e/a1

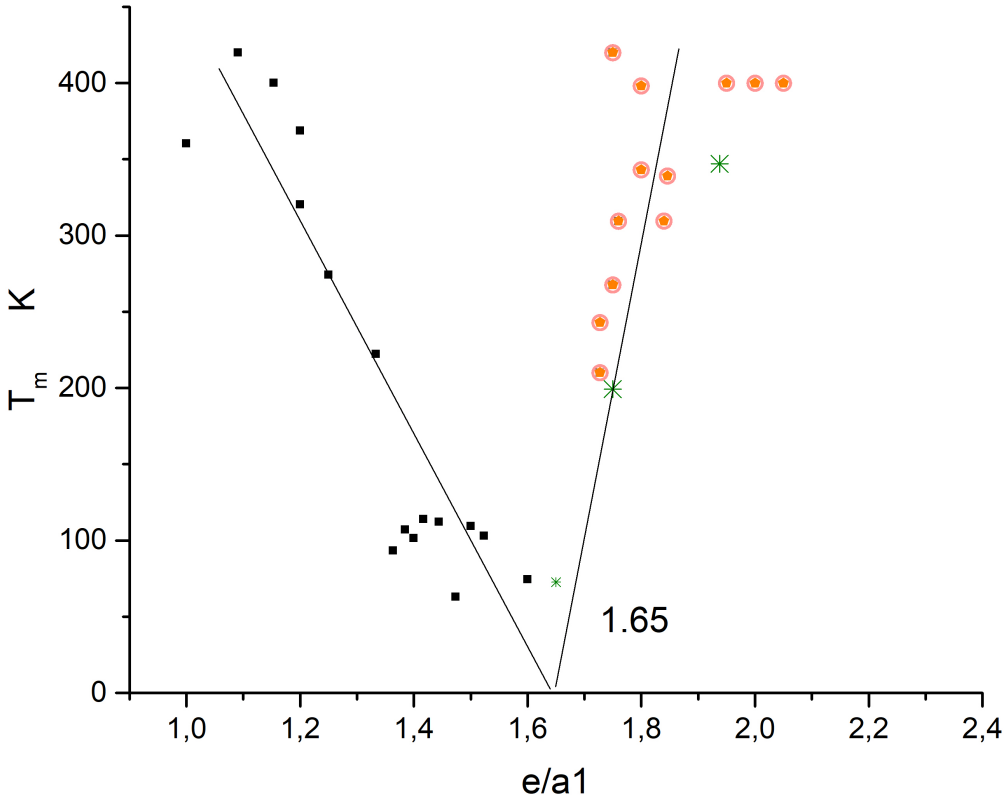

Highlights

- The Ni electronic structure [Ar] $3d^9$ $4s^1$ should be considered for Ni containing HEAs.
- The HEA phases Domains are: I-fcc e/a<1.53; II-mixed 1.53<e/a<1.88; III-bcc e/a>1.88.
- The Brillouin zone of HEAs has to be investigated in calculations and modelling.
- The average magnetic moment at saturation and the phases can be predicted for HEAs.

Declaration of interests

☒ The authors declare that they have no known competing financial interests or personal relationships that could have appeared to influence the work reported in this paper.

☐The authors declare the following financial interests/personal relationships which may be considered as potential competing interests: